http://dx.doi.org/10.1016/j.msea.2019.138219

Investigation on the enhanced maximum strain rate sensitivity (*m*) superplasticity of Mg-9Li-1Al alloy by a two-step deformation method

H.P. Yang[a], X. Zhang[b], P. Chen[b], M.W. Fu[a,*], G.C. Wang[b] and S. To[c]

[a] Department of Mechanical Engineering, The Hong Kong Polytechnic University, Hung Hom, Kowloon, Hong Kong

[b] School of Aviation Manufacturing Engineering, Nanchang Hangkong University, Nanchang 330063, PR China

[c] Department of Industrial and Systems Engineering and State Key Laboratory of Ultra-precision Machining Technology, The Hong Kong Polytechnic University, Hung Hom, Kowloon, Hong Kong

* Corresponding Author / E-mail: mmmwfu@polyu.edu.hk, TEL: +852- 2766-5527

Abstract

A two-step superplastic deformation (SPD) approach was employed for the SPD of Mg-9Li-1Al (LA91) alloy. In the first SPD step, the constant velocity (Const*v*) and constant strain rate (CSR) SPD were adopted with the outcome elongation ranging from 50 to 250 %. The maximum strain rate sensitivity (Max*m*) SPD, in which the maximum *m* value is always maintained, was then employed in the second SPD step. The results show that the two-step SPD can greatly enhance the superplasticity of LA91 alloy. The largest elongation of 621.1 % was obtained by CSR-Max*m* SPD with the pre-elongation of 250 %, which is even better than the results of single-step Max*m* SPD by using grain-refined materials. In addition, the mechanisms of the two-step SPD are discussed and an in-depth understanding of the SPD of LA91 alloy is obtained. This research thus provides a feasible method for efficiently enhancing the plasticity of Mg-Li based alloys for making complex parts and structures with complicated local and multi-scaled features.

Keywords: Two-step superplastic deformation, Constant velocity SPD, Constant strain rate SPD, Maximum strain rate sensitivity (*m*) SPD, Mg-Li alloy

1. Introduction

There is great potential for Mg-Li alloys in various applications due to their low density, high stiffness-to-weight ratio and biodegradability, favored by plenty of fields like biomedical and military clusters [1-4]. However, the parts used in these areas generally have complicated structures, which requires a large deformation for making the parts. For Mg-Li alloys, with the increase of Li content, the original hexagonal-close-packed (HCP) structure of Mg is transformed into the body-centered-cubic (BCC) structure and the axial ratio of the hexagonal Mg lattice is reduced [5]. The existence of HCP structure, however, may still compromise the formability of the alloy due to few slip systems available in Mg [6]. Therefore, innovative manufacturing methods should be explored for fabrication of complex parts made of Mg alloys. The material used in this research is Mg-9Li-1Al (in wt%, LA91) alloy. It has a duplex structure with the co-existence of α (HCP) and β (BCC) phases.

Superplasticity can facilitate polycrystalline materials to have a large deformation with the elongation usually more than 400 % [7]. Therefore, complex parts and components with complicated geometries and local features can be made by using superplastic deformation (SPD). In tandem with this, the SPD of Mg-Li alloy is thoroughly studied and fully exploited. There are some attempts to explore the SPD of Mg-Li alloys. However, the prior research focus is more on investigating the refinement of material microstructure to achieve superplasticity. The approaches to change the microstructure of material mainly include equal channel angular extrusion (ECAE) [8, 9], high ratio extrusion [10], and friction-stir processing (FSP) [11]. Meanwhile, some researchers explored other approaches to realize the SPD of Mg-Li alloys, including high strain rate SPD [12], coarse grain SPD [13], and low temperature SPD [14]. However, few of them have tried on exploring different deformation modes of SPD. In our previous research [15], the maximum strain rate sensitivity (*m*) SPD (Max*m* SPD) was employed to investigate the SPD of LA91 alloy, and the maximum elongation of 563.7 % was achieved by using the material refined by ECAE. In this research, a more efficient two-step SPD method was explored to realize the SPD of LA91 alloy to avoid the time-consuming grain-refinement tailed for SPD.

The approach of Max*m* SPD was developed to extend the deformation limit of Ti-alloys [16, 17]. The rationale of Max*m* SPD, illustrated in **Fig. 1**, is to maintain the maximum *m* value throughout the whole SPD process by simultaneous and in-situ measurement of *m* value and dynamic control of strain rate. Since the higher *m* value, the better superplasticity, the

maximum *m* value during the SPD process is thus controlled and realized in such a way the best superplasticity is implemented. It is founded that the Max*m* SPD is more favored by the grain-refined materials than the coarse-grained materials with the as-extruded state, due to more equiaxed grains in the former material [15]. However, the grain refinement of ECAE is too costly and time-consuming. To avoid the prerequisite of grain refinement of materials for SPD, the stepped SPD method was explored by directly using the as-extruded LA91 alloy in this research, which has been well validated to be efficient in the SPD of Ti alloys [18-20]. The idea of stepped SPD is to divide the deformation into two SPD steps, such that a refined grain structure can be induced during the first step, which is favored by Max*m* SPD in the second step, as illustrated in **Fig. 2**. In the prior research of two-step SPD [18-20], the constant velocity (Const*v*) and the Max*m* SPD were selected for the first and second steps, respectively. In this study, both Const*v* and constant strain rate (CSR) SPD were adopted for the first step, followed by Max*m* SPD applied for the second step. It was proven that the CSR SPD is more efficient for the first SPD step. In this research, the maximum elongation of 621.1 % was obtained by using CSR-Max*m* SPD with the pre-elongation of 250 %, which is even larger than the result by using grain-refined material in single-step Max*m* SPD [15]. A pilot study has proven the feasibility of two-step SPD by using Mg-Li alloys [21]. In this research, an in-depth exploration of deformation and fracture mechanisms of Mg-Li alloys during the two-step SPD process was conducted in such a way to better exploit the maximum *m* superplasticity of the Mg-Li alloy.

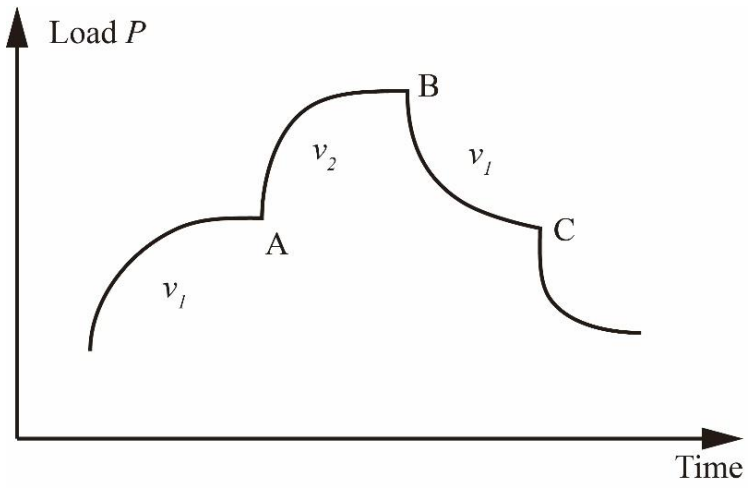

Fig. 1 Rationale for the Max*m* SPD [17].

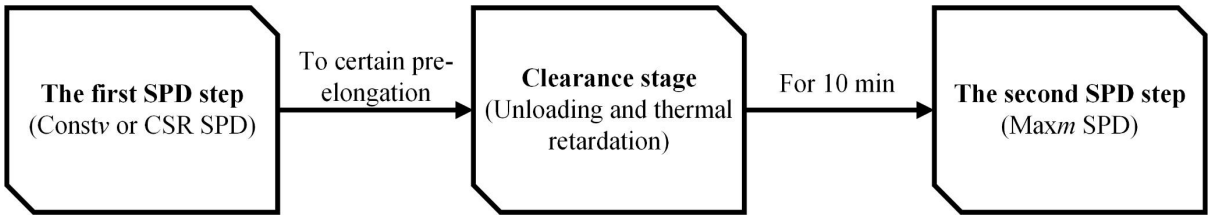

Fig. 2 The two-step SPD method

2. Experimental Procedures

2.1 Material Preparation

The as-received LA91 alloy with the as-extruded state was utilized in this study. The material was cast from pure Mg, Li, and Al powders with argon gas protection at first, and then extruded from the cast ingot at 563 K. The method of inductively coupled plasma optical emission spectrometer (ICP) was used to detect the material composition, showing that the alloy is composed of 8.829 % Li and 1.063 % Al (in wt %), which is very close to the theoretical value.

The as-extruded rods were then machined into dog bone specimens for SPD tensile tests with the gauge length of 15 mm and gauge diameter of 3 mm. The length direction of the specimen is parallel to the extrusion direction of the rod.

2.2 Single and two-step SPD Tensile Tests

The optimal SPD temperature for LA91 alloy is 573 K based on the prior research [15]. The apparatus for conducting the SPD tests is a tensile tester equipped with a resistance heating furnace. The tensile tester is controlled by a tailor-coded program to realize different SPD modes, including Const*v*, CSR and Max*m* SPD.

Single-step Const*v*, CSR and Max*m* SPD tests were first conducted to confirm the optimal process parameters of the LA91 alloy during SPD at the temperature of 573 K. The velocities of 0.195, 0.39, and 0.78 mm/min for Const*v* SPD and the strain rates of 0.00025, 0.0005, and 0.001 /s for CSR SPD were selected, such that the initial strain rate in Const*v* SPD is the same as the strain rate in CSR SPD. Meanwhile, the initial velocity v_0 = 0.07 mm/min, velocity increment Δv = 0.03 mm/min and time increment t = 6 s were used in Max*m* SPD

[15]. In each SPD experiment, the test started after the holding time of 10 min at 573 K in the furnace, and the samples were quenched upon completion of the experiments in such a way to preserve the microstructures at the SPD temperature. The optimal speed of 0.39 mm/min for Const*v* SPD and the optimal strain rate of 0.0005 /s for CSR SPD were then chosen based on the obtained elongation of the specimens.

The two-step SPD was then explored by using the optimal parameters. The elongations in the first and second steps are denoted as e_1 and e_2. The material was held for 10 min at 573 K at the beginning. Const*v* or CSR SPD was adopted in the first SPD step. After reaching the target e_1, the specimen was unloaded and 10 min of clearance stage was implemented, followed by the second step by using Max*m* SPD until fracture. Max*m* SPD was used in the second step because it can maintain the best superplastic state of the material until fracture, and the largest potential elongation can be attained. To explore the microstructural evolution during the first step, the observation of microstructure was done after e_1 from 50 to 250 % was obtained.

3. Results and Discussion

3.1 Single-step SPD experiments

Single-step SPD tests by using Const*v*, CSR and Max*m* SPD were conducted at the beginning of this research to determine the optimal process parameters of the alloy. The elongation obtained by using different SPD methods with various process parameters are summarized in **Fig. 3**. It can be observed that the elongation obtained by the lowest two velocities and strain rates in Const*v* and CSR SPD is similar, which is also the largest among the results obtained by using the same SPD method. The high velocity or strain rate does not provide enough time for dynamic recrystallization (DRX), which is the typical accommodation mechanism for grain boundary sliding (GBS) during SPD [22], such that fracture may occur at an early stage and the elongation can be compromised. Meanwhile, it can be obtained that larger elongation was generally achieved by Const*v* SPD, when the initial strain rate in Const*v* SPD is equal to the strain rate in CSR SPD. The speed remains unchanged in Const*v* SPD, but it keeps increasing in CSR SPD to maintain the constant strain rate, in this way the average speed in CSR SPD is higher. As a result, shorter elongation was achieved by CSR SPD, because the high deformation speed does not guarantee enough degree of DRX through SPD. Since the

lowest two velocities and strain rates in Const*v* and CSR SPD can lead to similar and the largest elongation among same SPD method, the velocity of 0.39 mm/min and the strain rate of 0.0005 /s were chosen as the optimal parameters for Const*v* and CSR SPD considering forming efficiency.

The deformed specimens after SPD by using the optimal process parameters are presented in **Fig. 4**, and the corresponding true stress-strain curves are shown in **Fig. 5**. In **Fig. 4**, diffusional necking can be found throughout the whole gauge length. It can be observed that the elongation by using Max*m* SPD is the largest among the three SPD methods, but it is not much better than the conventional methods of Const*v* and CSR SPD. This indicates that Max*m* SPD is not much more efficient than the conventional methods when the as-received material without grain refinement is used, which matches the finding in our previous research [15]. It can be observed in **Fig. 5** that the stress overshoots at the beginning in Const*v* and CSR SPD. Then, the stress drops rapidly, and the decreasing trend becomes gentle and finally even changes to a rising tendency. While for Max*m* SPD, the overshoot is suppressed, and the trend of the stress is steadier. In traditional SPD methods, the stress overshoot is resulted from strain hardening, which is caused by the movement and generation of dislocations [18]. As the deformation continues, strain energy is accumulated, which provides the source for DRX. As a result, the material is gradually softened by the enhanced GBS by DRX and enters the superplastic state. However, due to long-time exposure of the workpiece in the high-temperature environment, grain growth becomes severe, which hinders GBS and causes hardening of the material and rise in stress during deformation. In Max*m* SPD, the suppression of stress overshoot indicates that this method can facilitate faster entrance of the material into the superplastic state, which was achieved by continuously controlling the deformation speed to keep the maximum *m* value and the best superplastic state during SPD. Meanwhile, the undulatory curve in Max*m* SPD is caused by the continuous adjustment of the speed.

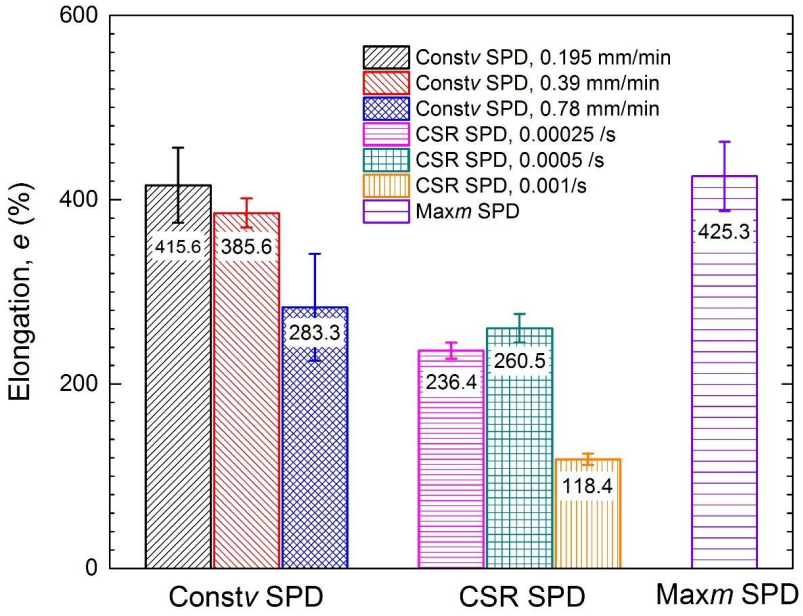

Fig. 3 The elongation results of single-step SPD experiments.

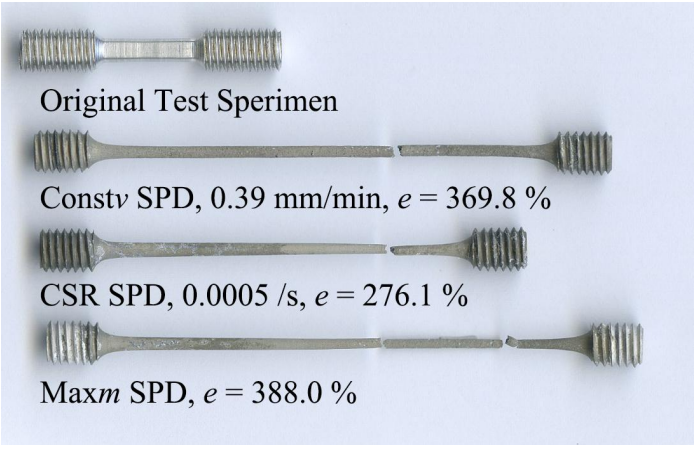

Fig. 4 Specimens after single-step tensile tests by different SPD methods.

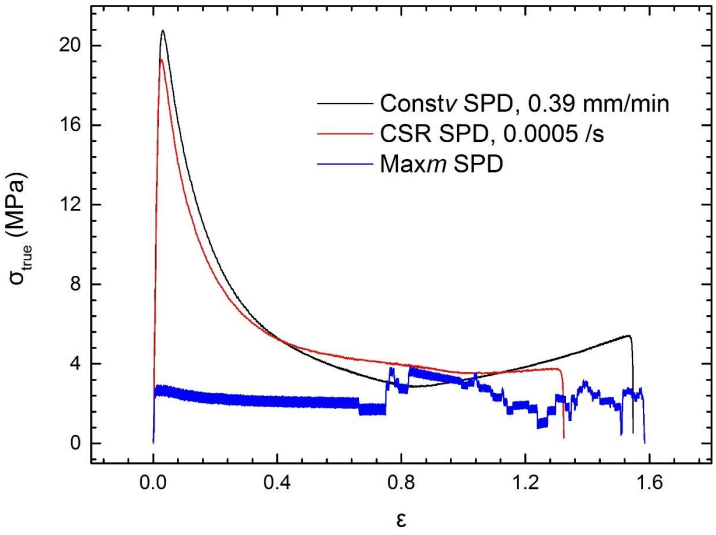

Fig. 5 True stress-strain curves of the single-step SPD tests by different methods.

3.2 Two-step SPD experiments

Two-step SPD tests were conducted by using Const*v*-Max*m* and CSR-Max*m* SPD methods. The optimal parameters of velocity of 0.39 mm/min and the strain rate of 0.0005 /s were employed in Const*v* and CSR SPD, respectively. The deformed samples after the two-step tests are shown in **Fig. 6**, and it can be found that the two-step method can largely extend the deformation limit of the material compared to single-step method. The largest elongation by using the two-step method is 621.1 %, obtained by CSR-Max*m* SPD with e_1 of 250 %, which is even larger than the optimum elongation of 563.7 % achieved by single-step Max*m* SPD with the application of ECAE-processed LA91 alloy [15]. This indicates that the two-step method is more efficient than the application of grain refinement process in terms of inducing better superplasticity. It can be noted that by using Const*v*-Max*m* SPD, the final elongation is increased with e_1 from 50 to 200 %, but the elongation becomes decreased when e_1 is greater than 200 %. However, the overall elongation by using CSR-Max*m* SPD is generally increased with e_1 from 50 to 250 %. Meanwhile, the variation of e_2 with different e_1 is summarized in **Fig. 7**. For Const*v*-Max*m* SPD, as e_1 is increased from 50 to 150 %, e_2 generally increases. After a plateau for e_1 from 150 to 200 %, e_2 decreases dramatically when e_1 reaches 250 %. However, for CSR-Max*m* SPD, the e_2 is increased with e_1 from 50 to 150 % but remains steady when e_1 is larger than 150 %. Therefore, the variation of the overall elongation is mainly due to the change in e_2, which indicates that the superplasticity during Max*m* SPD is improved with the increase of e_1 when e_1 is small. However, when e_1 is larger than 150 %, the increase of e_1 cannot further enhance the superplasticity in the second SPD step. Meanwhile,

the different variation trends of e_2 by using Const*v* and CSR SPD after e_1 reaches 150 % implies the different microstructure evolution processes during the two methods, which will be discussed in the following text.

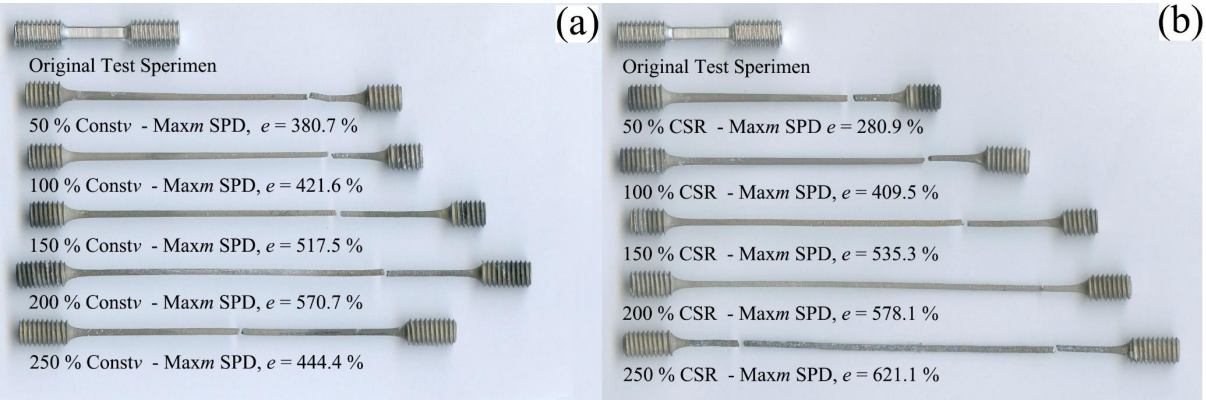

Fig. 6 Samples deformed by (a) Const*v*-Max*m* and (b) CSR-Max*m* SPD with different e_1.

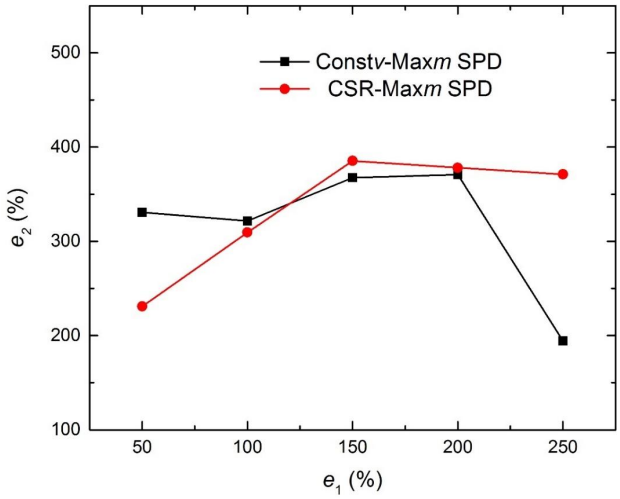

Fig. 7 Summary of second-step elongation with different e_1 by using different SPD methods.

The true stress-strain curves of two-step SPD tests, which are combined by single-step curves of Const*v* or CSR SPD in the first step and Max*m* SPD in the second step, are shown in **Fig. 8**. It can be observed that when e_1 is smaller than 150 %, the curves of Max*m* SPD in the second step is generally steady or rises slightly, which is similar to the case of single-step Max*m* SPD in **Fig. 5**. However, when e_1 exceeds 150 %, the rising trend of the stress in Max*m* SPD curve becomes more obvious. Meanwhile, it can also be noted that for Const*v*-Max*m* SPD, the initial stress of the second SPD step with e_1 of 250 % is higher than that with e_1 of 200 %. While for CSR-Max*m* SPD, the initial stresses of the second step with e_1 of 200 and 250 % are almost the same. This also implies different microstructural

evolution behaviors during the first step in the two SPD methods.

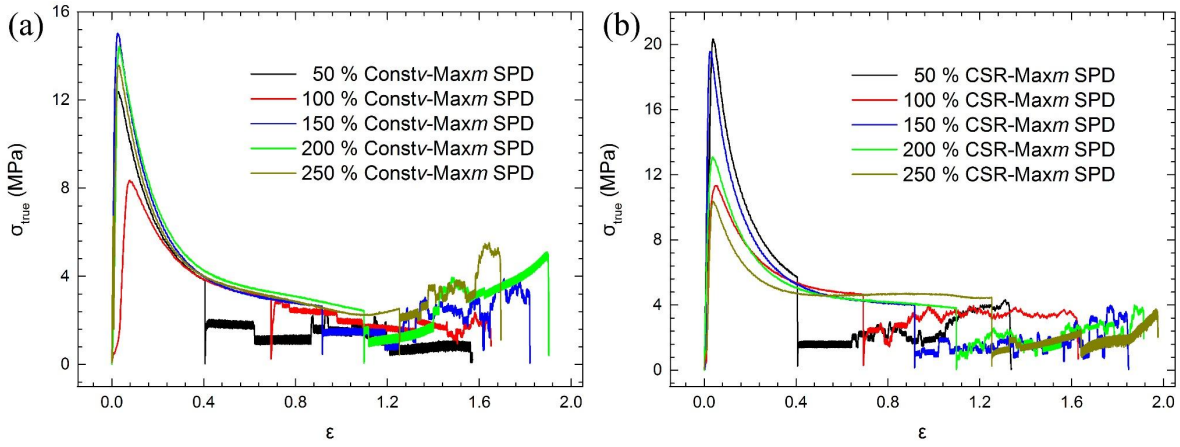

Fig. 8 True stress-strain curves of two-step SPD tests by (a) Const*v*-Max*m* SPD and (b) CSR-Max*m* SPD.

In order to investigate the microstructure evolution during the first SPD step, some specimens were collected after the first SPD step, whose microstructures were prepared as shown in **Figs. 9 and 10**. The samples were prepared by grinding and polishing along the longitudinal direction to mirror surface and etching with 5 % HNO_3 water solution for 3-4 s to expose different phases and grain boundaries, which were then observed by an optical microscope. In **Figs. 9 and 10**, the α phase, which is white with the HCP structure, is distributed in the background β phase matrix, which is darker with the BCC structure [23]. In the as-received material with the as-extruded state, the α phase is strip-like and elongated owing to severe deformation during extrusion. This microstructure with the nonhomogeneous and tremendously long α phase strips is not favored by Max*m* SPD [15]. However, after the first deformation step by using Const*v* or CSR SPD, the strips of α phase gradually disappear and are replaced by finer and more equiaxed grains, which are generated by DRX during the SPD process. With the increase of e_1 by using CSR SPD, the overall α phase grains after the first SPD step are still equiaxed with many newly-emerged little α phase grains. However, during Const*v* SPD, the α phase grains after the first SPD step become more linked and integrated as e_1 is increased.

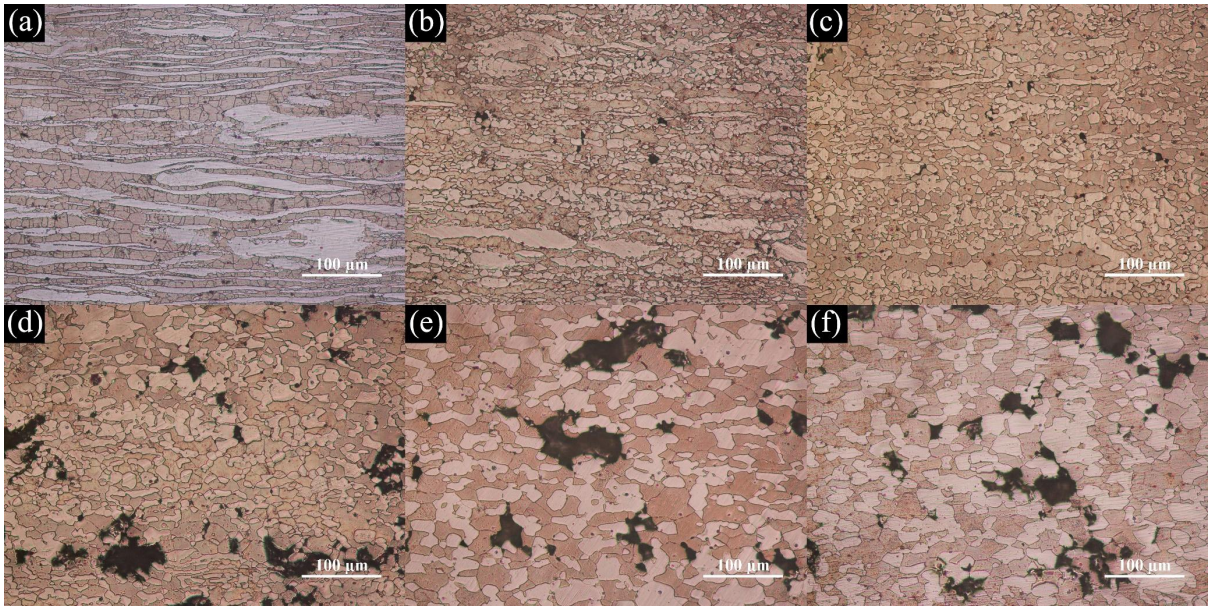

Fig. 9 Microstructures of the LA91 specimens with the material states of (a) as-extruded and deformed after the pre-elongation of (b) 50 %, (c) 100 %, (d) 150 %, (e) 200 %, and (f) 250 % in Const*v*-Max*m* SPD.

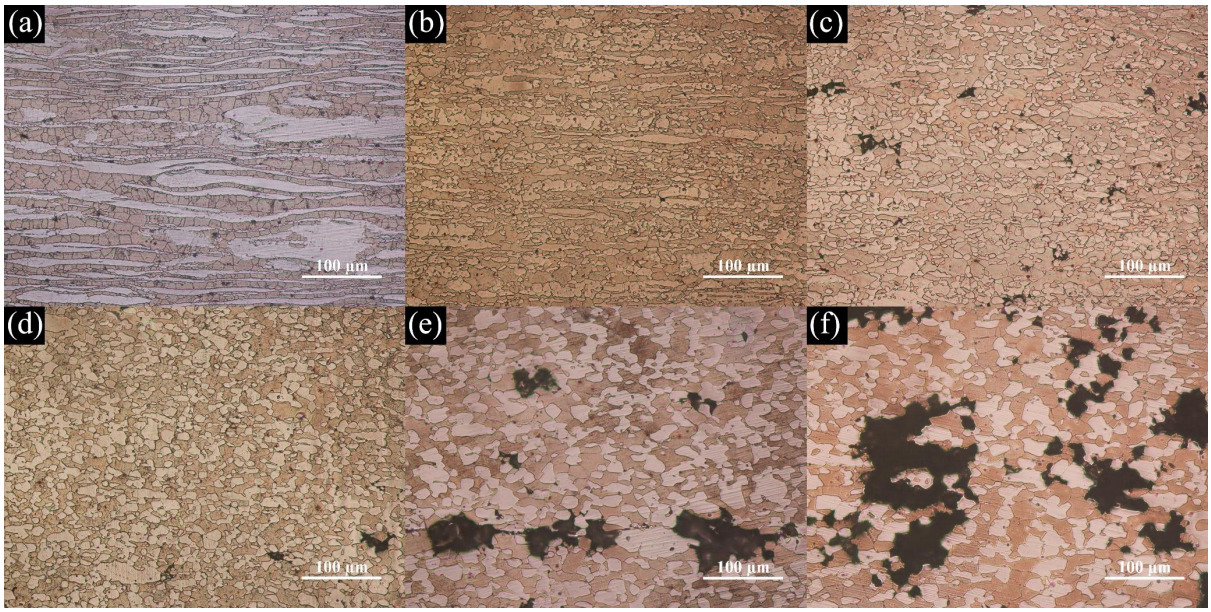

Fig. 10 Microstructures of the LA91 specimens with the material states of (a) as-extruded and deformed after the pre-elongation of (b) 50 %, (c) 100 %, (d) 150 %, (e) 200 %, and (f) 250 % in CSR-Max*m* SPD.

For further revealing the material microstructure evolution during the first SPD step, the technique of electron back scatter diffraction (EBSD) was utilized for the raw material and

deformed samples after the first SPD step, as shown in **Fig. 11**. It can be observed that the β phase area is black, which indicates that the Kikuchi pattern in the β phase cannot be well indexed. A possible explanation is that the β phase in the Mg-Li alloy is somehow softer than the α phase, which leads to high concentration of deformation and dislocation density. As a result, lattice perfection in the β phase is low, and the β phase cannot be clearly indexed by EBSD [11]. In the as-extruded material, the long α phase strips are composed of many subgrains with low angle boundaries. While during the first SPD step, the subgrains gradually disappear, and the equiaxed grains with more high angle boundaries emerge. The grain sizes measured by using the EBSD software in **Fig. 11 (b)-(e)** are 6.5, 10.9, 5 and 5.6 μm, respectively. It can be obtained that the grains during Const*v* SPD have increased, while the average grain size remains almost the same during the CSR SPD process. In fact, there exist some large grains after the first SPD step with e_1 of 250 % in CSR SPD, but because of many newly-formed small grains, the overall grain size can remain almost unchanged. Meanwhile, the misorientation angles of the boundaries were calculated and summarized in **Fig. 11**. It can be observed that the portion of high angle grain boundaries (HAGBs) is decreased with the increase of e_1 by Const*v* SPD, but the HAGB portion is greatly increased in the CSR SPD process. The increase in HAGBs during CSR SPD indicates that many recrystallized grains have been formed by DRX [24], which is more beneficial for the second SPD step by using Max*m* SPD.

For single-step Max*m* SPD or two-step SPD methods with small e_1, exposure time of the material in high-temperature environment is short and the grain size is still relatively small. However, after the application of large e_1 ($\geqslant$ 150 %), grain coarsening becomes more significant and cavities begin to form, as shown in **Figs. 9 and 10**. Therefore, the different stress fluctuation patterns of Max*m* SPD in **Fig. 8** are caused by the distinction in grain sizes of the material. For the alloy with a smaller average grain size, Max*m* SPD can facilitate the material to maintain the best superplastic state by adjustment of deformation speed, so the stress can be kept steady. However, if the grain size is large and there exist cavities in the material, GBS in the alloy is hindered and hardening becomes more obvious, such that the superplastic state of the material is compromised. In this way, the hardening effect becomes dominant during Max*m* SPD, which causes the rising trend of stress. Similarly, the higher initial stress in the second step of Const*v*-Max*m* SPD with e_1 of 250 % than that with e_1 of 200 % is caused by the larger and more linked grain structure in the former case. While the

similar initial stresses in the second step of CSR-Max*m* SPD with e_1 of 200 and 250 % are due to the similar grain structures in the materials. Meanwhile, the hardening in the second step of CSR-Max*m* SPD is not as significant as that in Const*v*-Max*m* SPD, which could also be attributed to the larger average grain size obtained after Const*v* SPD.

The differences in microstructural evolution in Const*v* and CSR SPD are caused by different deformation modes in these two methods. CSR SPD has a higher average speed, and a shorter forming time is required for achieving the same e_1. Therefore, with the same e_1, the grain structure after CSR SPD is finer and more homogenized compared to Const*v* SPD due to less grain growth. This becomes more obvious as e_1 increases, because the difference between the average speeds of Const*v* and CSR SPD is also larger. As a result, the distinction in forming time between e_1 of 200 and 250 % is smaller for CSR SPD compared with Const*v* SPD, and grain coarsening effect is severer in Const*v* SPD. However, if a higher deformation speed is applied directly to Const*v* SPD, earlier fracture might occur. This is because the speed is gradually accelerated in CSR SPD, and the initial speed is low. As a result, the strain hardening effect is not obvious, and the deformation is accelerated after the material enters the superplastic state. While for Const*v* SPD using high speed, strain hardening causes severer stress overshooting, and the material cannot enter the superplastic state well, so the superplasticity and final elongation might be compromised. Therefore, the microstructure with more recrystallized grains and relatively small average grain size is more favored by Max*m* SPD in the second SPD step, which can be better achieved by CSR SPD with a low strain rate.

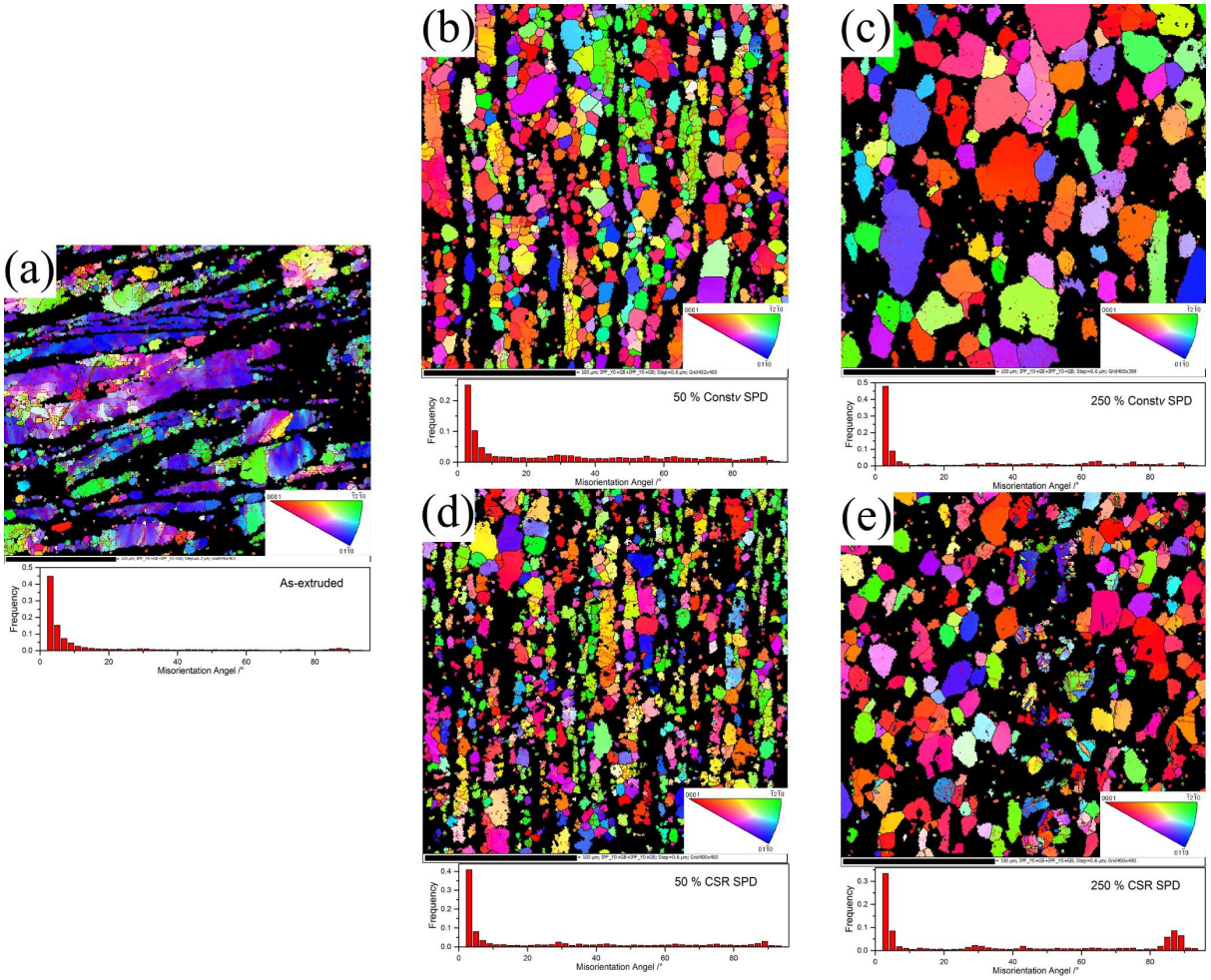

Fig. 11 EBSD graph of the specimens (a) with as-extruded state, and deformed after (b) 50 % Const*v* SPD, (c) 250 % Const*v* SPD, (d) 50 % CSR SPD, and (e) 250 % CSR SPD.

3.3 *m* value variation analysis

The *m* value is an indicator for the superplastic state during SPD, and a larger *m* value can generally indicate a better superplastic state. In this research, to study the variation of *m* value during the second step of deformation by using Max*m* SPD, the *m* value-true strain curves of the deformation processes are plotted in **Fig. 11**. As the Max*m* SPD process is inherently continuously changing the deformation strain rate, the *m* value during each abrupt change of strain rate can be theoretically calculated by following equations [14] with the parameters shown in **Fig. 1**. Since the *m* value varies violently, the averages of every 20 derived *m* values were used to plot the graph to smoothen the curves.

$m = \log (P_B / P_A) / \log (v_2 / v_1)$, for increased strain rate,

$m = \log (P_B / P_C) / \log (v_2 / v_1)$, for decreased strain rate,

where P_A, P_B, and P_C are the loading force at A, B, and C points, and v_1 and v_2 are the deformation speeds during the adjacent time increments, where v_2 refers to the higher speed and v_1 refers to the lower one in **Fig. 1**. The initial strain is different in each curve in **Fig. 12**, because the curves only present the variation of m value during Max$m$ SPD in the second SPD step and e_1 in each experiment is different.

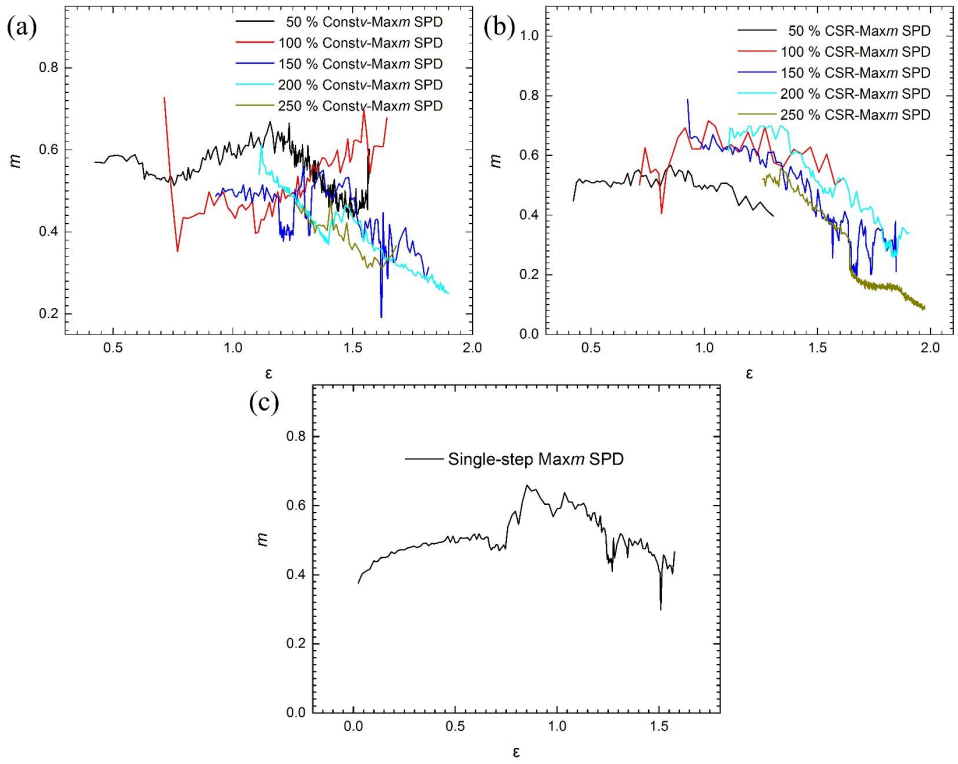

Fig. 12 m value variation in the second step of (a) Const$v$-Max$m$ SPD and (b) CSR-Max$m$ SPD, and (c) Single-step Max$m$ SPD.

It can be observed that for small e_1 (< 150 %), the m value fluctuates around the same level during SPD. However, the m value for the larger e_1 (⩾ 150 %) shows a decreasing tendency, and the m values at the end of the SPD tests which achieved the largest elongation by both Const$v$-Max$m$ and CSR-Max$m$ SPD are also the smallest among the same SPD method. The declining trend of m value when e_1 is greater than 150 % indicates that the best superplastic state is achieved at the beginning of Max$m$ SPD, and the superplastic state gradually deteriorates until fracture. As shown in **Figs. 9 and 10**, when e_1 is larger than 150 %, grains are coarsened, and cavities begin to form in the alloy. As the deformation continues in the second step, grain growth and cavity formation become severer, so GBS during the SPD process is more hindered, which results in a compromised superplastic state in the material

and a smaller *m* value. For two-step tests which achieved the largest final elongation, the exposure time for the material in the high-temperature environment is also the longest, and grain growth and cavity formation are the severest among the same deformation method, the *m* value at the final stage is therefore the lowest. However, when e_1 is small (< 150 %), the *m* value is more stable, which is very similar to the single-step Max*m* SPD curve shown in **Fig. 12 (c)**. This indicates that small e_1 (< 150 %) does not much change the material state in terms of *m* value variation, while the material state is deteriorated for large e_1 ($\geqslant$ 150 %), which leads to the decreasing *m* value. This could also be a possible reason for the variation of e_2 shown in **Fig. 7**, in which the rising trend of e_2 is terminated when $e_1 \geqslant$ 150 %. The decreasing trend of *m* value when $e_1 \geqslant$ 150 % indicates the gradually deteriorated superplastic state during deformation, so the e_2 cannot be increased further due to the inferior grain structure.

3.4 Fracture Mechanisms

To analyze the microstructure evolution near the fracture region, microstructures of 6 mm from fracture region of specimens after two-step SPD with e_1 of 50, 200 and 250 % were first prepared, as shown in **Fig. 13**. The e_1 of 50, 200 and 250 % were selected because they correspond to the smallest and largest overall elongation in the two-step SPD tests. It can be noticed that the microstructure after the second SPD step is completely different compared to the first SPD step, and both the α and β phase grains have grown and more cavities are formed inside the material. As shown in **Fig. 13 (a) and (d)**, for the material which achieved the smallest final elongation with e_1 of 50 %, the α and β phases are relatively uniformly distributed. However, when e_1 reaches 200 and 250 %, which led to the largest two elongation among the same SPD method, the α phase tends to merge and an increased proportion of the α phase can be observed. Meanwhile, for the material which obtained the largest elongation by using the same SPD method in **Fig. 13 (b) and (f)**, the proportion of the α phase in the alloy is higher than that in the material which achieved the second largest elongation in **Fig. 13 (c) and (e)**.

The fracture region microstructures of the deformed samples with the largest two final elongation among the same SPD method were also prepared, as shown in **Fig. 14**. Compared to microstructure far from the fracture, the proportion of α phase in the fracture region has much increased. Moreover, it can be observed that the portion of α phase is higher for larger final elongation. It was inferred that for the LA91 alloy, stress-induced transformation in

which the β phase is transformed into the α phase could occur near the fracture region, because of a higher level of stress suffered near the fracture region [15]. Fracture during SPD is caused by the coalescence of cavities formed inside the alloy during deformation, and it can be noticed in **Figs. 13 and 14** that the cavities are mainly formed inside the α phase or at the boundaries between α and β phases. The α phase with the HCP structure tends to fracture more easily than the β phase with the BCC structure, so it can be inferred that the β phase is transformed into α phase such that fracture could occur inside the α phase. When larger final elongation is obtained, more β phase can be transformed into the α phase, and a higher proportion of the α phase in the alloy can be generated and induced. The final elongation, therefore, largely depends on how the deformation method can prevent the α phase from cavitation and fracture.

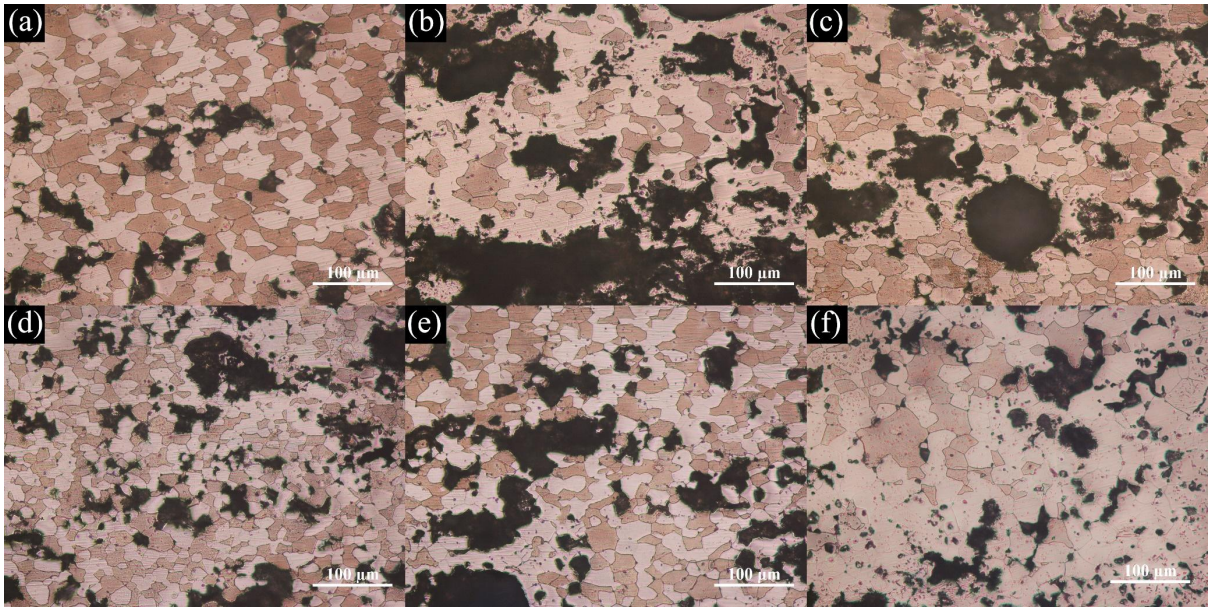

Fig. 13 Microstructures which are about 6 mm from the fracture regions of specimens after SPD tensile tests by methods of (a) 50 % Const*v*-Max*m* SPD, (b) 200 % Const*v*-Max*m* SPD, (c) 250 % Const*v*-Max*m* SPD, (d) 50 % CSR-Max*m* SPD, (e) 200 % CSR-Max*m* SPD, and (f) 250 % CSR-Max*m* SPD.

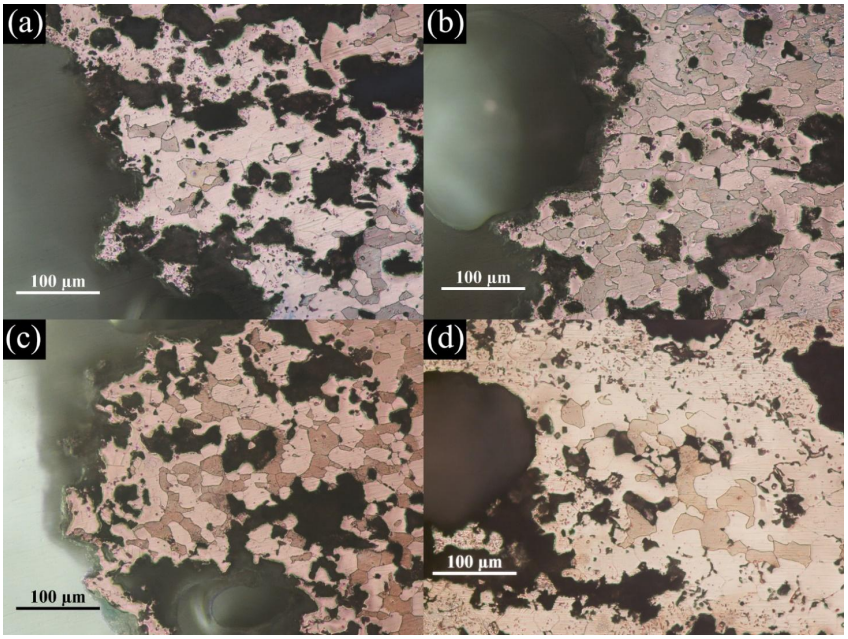

Fig. 14 Microstructures of fracture regions of the specimens after SPD tensile tests by the methods of (a) 200 % Const*v*-Max*m* SPD, (b) 250 % Const*v*-Max*m* SPD, (c) 200 % CSR-Max*m* SPD, and (d) 250 % CSR-Max*m* SPD.

The overall material microstructure of about 6 mm from fracture is shown in **Fig. 15**, which shows the cavity distribution in the material near fracture. Since the cavities are linked and it is difficult to measure the single cavity size, the proportion of the cavity inside the material (or porosity) was measured and calculated by image analyzing software, as shown in **Fig. 16**. For the specimens which achieved larger elongation, more long and coalesced cavities exist in the microstructure, and the level of porosity is also the highest. It was found in *m* value variation analysis that the *m* value shows a decreasing trend and the smallest *m* value is obtained at the end of the deformation process when e_1 is large. The high level of porosity could be one of the reasons for the lowest *m* value, because cavities formed in the metal can hinder GBS and deteriorate the superplasticity. Nevertheless, the largest elongation can still be achieved even if the *m* value is small. During the first step of the two-step SPD method, the material can be efficiently deformed with relatively high speed, and more strain energy can be generated which can facilitate DRX. In this way, although the increased e_1 from 150 to 250 % does not further increase e_2 due to grain growth and cavity formation, the overall elongation has already been increased. Therefore, the two-step SPD method can reach a larger elongation probably because it can postpone fracture of the material by efficiently obtaining pre-elongation and maintaining the best superplastic state by Max*m* SPD in the

second SPD step.

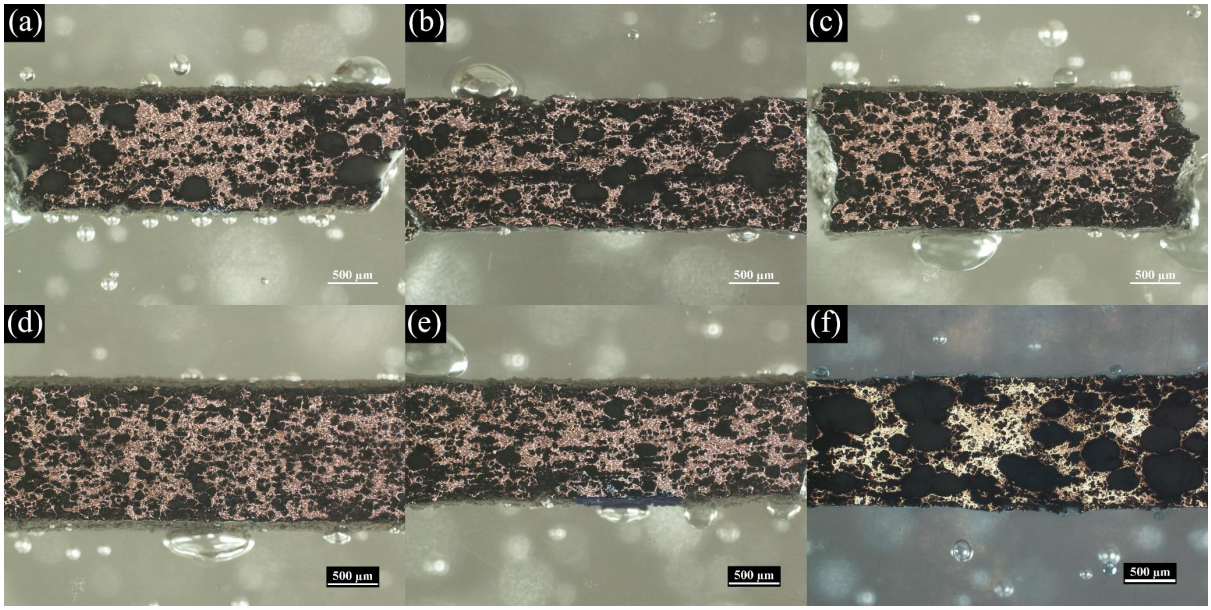

Fig. 15 Overall inner structure of about 6mm from the fracture regions of the specimens after SPD tensile tests by the methods of (a) 50% Const*v*-Max*m*SPD, (b) 200% Const*v*-Max*m*SPD, (c) 250% Const*v*-Max*m*SPD, (d) 50% CSR-Max*m*SPD, (e) 200% CSR-Max*m*SPD, and (f) 250% CSR-Max*m*SPD.

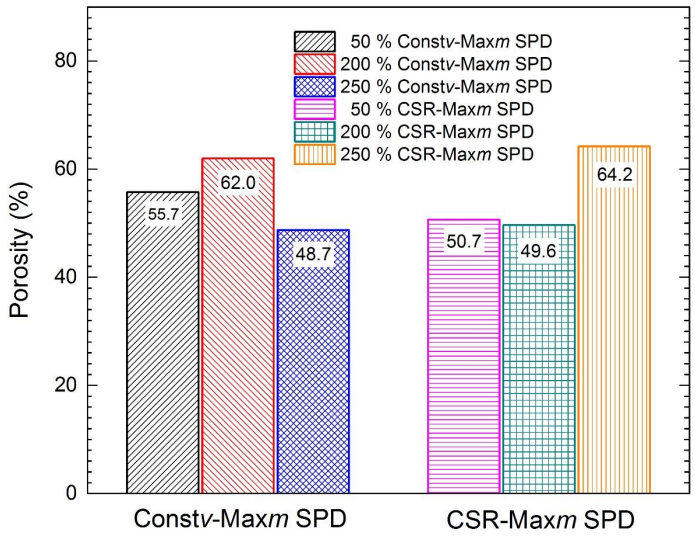

Fig. 16 Porosity of the samples in **Fig. 15**.

4. Conclusions

The two-step superplastic deformation (SPD) method was applied to the LA91 alloy to investigate its applicability in achieving large deformation in Mg-Li alloys for making complex structures. For this approach, the single-step SPD by using constant velocity (Const*v*), constant strain rate (CSR) and maximum strain rate sensitivity (Max*m*) SPD were conducted first to search for the optimum parameters and suitable pre-elongation. Two-step tests by using Const*v*-Max*m* and CSR-Max*m* SPD were then explored. From this research, the following conclusions can be derived and summarized as follows.

- The largest elongation of 621.1 % was obtained by the as-extruded material by using CSR-Max*m* SPD with the pre-elongation of 250 %, and the two-step method is more efficient than the application of grain refinement in terms of inducing superplasticity.
- The pre-elongation step in the two-step method can gradually change the long α phase strips into more equiaxed grains, and the optimized microstructure can lead to larger overall elongation.
- Generally, CSR SPD is more efficient than Const*v* SPD when applied in the first SPD step, because of higher average velocity and the lower level of grain growth in the microstructure.
- When the pre-elongation is greater than 150 %, the elongation in the second step by using Max*m* SPD is not further increased, and the *m* value becomes decreased throughout the Max*m* SPD process, which is because the elongated grains have been fully transformed into equiaxed grains by dynamic recrystallization, and grain growth and cavity formation become dominant when larger pre-elongation is obtained.
- For the largest final elongation, the highest proportion of α phase and porosity level can be found in the material. In addition, cavities are almost generated within the α phase and between the boundaries between α and β phases, because the α phase with the hexagonal-close-packed (HCP) structure tends to be fractured much easier. Meanwhile, two-step method can postpone fracture by efficiently obtaining pre-elongation and maintaining the best superplastic state by Max*m* SPD in the second step.

Acknowledegments

This work was funded by the G-YBL2 project from the Hong Kong Polytechnic University and the State Key Laboratory of Ultra-precision Machining Technology. We would also express our sincere appreciation to our colleagues and friends in the School of Aviation Manufacturing Engineering in Nanchang Hangkong University who provided great assistance in both the theory and experiments in this research.

Data Availability

The raw/processed data required to reproduce these findings cannot be shared at this time because these data will be used for further analysis in our research in the future.

References

[1] W.R. Zhou, Y.F. Zheng, M.A. Leeflang, J. Zhou, Mechanical property, biocorrosion and in vitro biocompatibility evaluations of Mg–Li–(Al)–(RE) alloys for future cardiovascular stent application, Acta Biomaterialia 9(10) (2013) 8488-8498.

[2] J.R. Nebeker, R. Virmani, C.L. Bennett, J.M. Hoffman, M.H. Samore, J. Alvarez, C.J. Davidson, J.M. McKoy, D.W. Raisch, B.K. Whisenant, Hypersensitivity cases associated with drug-eluting coronary stents: a review of available cases from the Research on Adverse Drug Events and Reports (RADAR) project, Journal of the American College of Cardiology 47(1) (2006) 175-181.

[3] T. Wang, M. Zhang, R. Wu, Microstructure and properties of Mg–8Li–1Al–1Ce alloy, Materials Letters 62(12–13) (2008) 1846-1848.

[4] Z. Wen, C. Wu, C. Dai, F. Yang, Corrosion behaviors of Mg and its alloys with different Al contents in a modified simulated body fluid, Journal of Alloys and Compounds 488(1) (2009) 392-399.

[5] F. Hauser, P. Landon, J. Dorn, Deformation And Fracture of Alpha Solid Solutions of Lithium In Magnesium. Technical Report No. 4, California. Univ., Berkeley. Minerals Research Lab., 1956.

[6] D. Poerschke, The Effects of forging on the microstructure and tensile properties of magnesium alloys AZ31 and ZK60, Case Western Reserve University, Cleveland, OH, USA (2009).

[7] M. Kawaski, T.G. Langdon, Superplasticity in ultrafine-grained materials, Reviews on

Advanced Materials Science 54 (2018) 46-55.

[8] M. Furui, C. Xu, T. Aida, M. Inoue, H. Anada, T.G. Langdon, Improving the superplastic properties of a two-phase Mg–8% Li alloy through processing by ECAP, Materials Science and Engineering: A 410–411 (2005) 439-442.

[9] Y. Yoshida, L. Cisar, S. Kamado, Y. Kojima, Low temperature superplasticity of ECAE processed Mg-10% Li-1% Zn alloy, Materials Transactions 43(10) (2002) 2419-2423.

[10] S.L. Dong, T. Imai, S.W. Lim, N. Kanetake, N. Saito, I. Shigematsu, Superplasticity in Mg-Li-Zn alloys processed by high ratio extrusion, Materials and Manufacturing Processes 23(3-4) (2008) 336-341.

[11] F.C. Liu, M.J. Tan, J. Liao, Z.Y. Ma, Q. Meng, K. Nakata, Microstructural evolution and superplastic behavior in friction stir processed Mg-Li-Al-Zn alloy, Journal of Materials Science 48(24) (2013) 8539-8546.

[12] X. Liu, G. Du, R. Wu, Z. Niu, M. Zhang, Deformation and microstructure evolution of a high strain rate superplastic Mg–Li–Zn alloy, Journal of Alloys and Compounds 509(39) (2011) 9558-9561.

[13] K. Lin, Z. Kang, Q. Fang, J. Zhang, Superplasticity at Elevated Temperature of a Coarse-Grained Mg–Li Alloy, Advanced Engineering Materials 16(4) (2014) 381-388.

[14] K. Edalati, T. Masuda, M. Arita, M. Furui, X. Sauvage, Z. Horita, R.Z. Valiev, Room-temperature superplasticity in an ultrafine-grained magnesium alloy, Scientific reports 7(1) (2017) 2662.

[15] H.P. Yang, M.W. Fu, S. To, G.C. Wang, Investigation on the maximum strain rate sensitivity (m) superplastic deformation of Mg-Li based alloy, Materials & Design 112 (2016) 151-159.

[16] G. Wang, M.W. Fu, Maximum m superplasticity deformation for Ti–6Al–4V titanium alloy, Journal of Materials Processing Technology 192–193 (2007) 555-560.

[17] G.C. Wang, M.W. Fu, C.X. Cao, H.B. Dong, Study on the maximum m superplasticity deformation of Ti–6.5Al–3.5Mo–1.5Zr–0.3Si alloy, Materials Science and Engineering: A 513–514 (2009) 32-41.

[18] X. Xu, G. Wang, C. Xia, Stepped superplasticity deformation-induced plastic enhancement of Ti–6Al–1.5Cr–2.5Mo–0.5Fe–0.3Si alloy, Materials & Design 36 (2012) 136-140.

[19] Q.J. Sun, G.C. Wang, M.Q. Li, Enhanced the superplasticity in Ti–6.5Al–2Zr–1Mo–1V alloy by a two-step deformation method, Materials & Design 35 (2012) 80-86.

[20] X.F. Xu, J.G. Zhang, C.F. Liu, G.C. Wang, Z.H. Yun, Superplastic Behaviour and Microstructural Evolution in Stepped Tensile Deformation of Titanium Alloy, Journal of Materials Engineering and Performance 23(1) (2014) 187-192.

[21] M. Fu, H. Yang, P. Chen, X. Zhang, G. Wang, Study on the Enhanced Superplasticity of Mg-Li Based Alloy by a Stepped Deformation Method, Defect and Diffusion Forum, Trans Tech Publ, 2018, pp. 103-108.

[22] M.E. Kassner, Fundamentals of creep in metals and alloys, Butterworth-Heinemann2015.

[23] M. Zhang, F. Elkin, Magnesium–Lithium Superlight Alloys, Beijing: Science Press, 2010.

[24] A.D. Rollett, Applications of Texture Analysis, John Wiley & Sons2008.